

Mechanism of Oxidation of Brilliant Cresyl Blue with Acidic Chlorite and Hypochlorous Acid. A Kinetic Approach

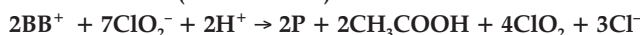
Lindelani Qwabe, Brijesh Pare and Sreekanth B. Jonnalagadda*

School of Chemistry, University of KwaZulu-Natal, Westville Campus, Durban, 4000 South Africa.

Received 3 December 2004; revised 27 April 2005; accepted 9 June 2005.

ABSTRACT

The kinetics and mechanism of oxidation of brilliant cresyl blue (7-amino-3-diethylamino-8-methyl-phenoxazine chloride) (BB^+) by chlorite in the presence of acid is reported. Under $[\text{H}^+]_0 > [\text{ClO}_2^-]_0 > [\text{BB}^+]_0$ conditions, the oxidation reaction followed *pseudo* first-order kinetics with respect to BB^+ . During the reaction, chlorite ion disproportionates, resulting in accumulation of chlorine dioxide. The overall reaction is third-order with first-order dependence on both H^+ and ClO_2^- ions. The rate coefficient for the overall reaction is $(0.158 \pm 0.003) \text{ l}^2 \text{ mol}^{-2} \text{ s}^{-1}$. The stoichiometry of the reaction is



where P = 7-amino-3-ethylamino-8-methyl-phenoxazine-10-N-oxide, and it varied with the initial concentrations of chlorite and acid. Near neutral pH, the hypochlorite-initiated oxidation of BB^+ proceeded through two second-order pathways, one driven by OCl^- ion and the other by HOCl . The latter reaction is much faster, with $k = (1.26 \pm 0.04) \times 10^3 \text{ l mol}^{-1} \text{ s}^{-1}$. At low pH, the reaction was much faster and had first-order dependence on the concentrations of BB^+ , H^+ and HOCl . Ru(III) catalysed the BB^+ -chlorite reaction with efficiency and the kinetics of the catalysed reaction are reported. Ru(III) had a catalytic constant, $k_{\text{CAT}} = 1.2 \times 10^6 \text{ l}^3 \text{ mol}^{-3} \text{ s}^{-1}$. The activation parameters for both uncatalysed and catalysed reactions were also reported. The kinetic profiles of the title reaction were computed using the proposed 11-step mechanism and Simkine software. The simulated curves agreed well with the experimental curves.

KEYWORDS

Kinetics, reaction mechanisms, dyes, water chemistry, computer chemistry.

1. Introduction

The chlorite ion has been the subject of extensive studies due to its interesting chemistry of disproportionation into chlorine dioxide and chloride, plus chlorate or hypochlorite depending on pH conditions, and due to the associated scope for excitability and exotic non-linear kinetic patterns.^{1,2} Further, chlorite is also widely used as a disinfectant and in water treatment.³ Many heterocyclic and triaryl compounds from chemical and other industrial processes end up in the water systems. Thus, the reactions of chlorite with various organic species, particularly the organic dyes used in various industries that enter water systems, are of concern and of interest from the public health point of view. Brilliant cresyl blue (7-amino-3-diethylamino-8-methyl-phenoxazine chloride) (BB^+), a heterocyclic species which is used in the staining of bone marrow smears, reticulocytes and trichomonads,⁴ belongs to the phenoxazine class of dyes. This cationic dye, which is stable and water-soluble with an absorption peak at 622 nm, was chosen as a representative species for the studies. Preliminary studies indicated that the kinetic profiles of BB^+ depletion depended significantly on the initial concentrations of acid and chlorite. This communication reports the elucidated mechanism of the reaction of BB^+ with acidic chlorite and hypochlorous acid by following a kinetic approach.

2. Experimental

2.1. Reagents

Brilliant cresyl blue (Aldrich) was used as supplied. Sodium chlorite (BDH) was recrystallized before use.⁵ All the other reagents used were of Analar or high purity grade. Owing to the

observed high sensitivity of reaction rates to the pH, all the solutions were made in distilled water and deionized ultrapure water.

2.2. Hypochlorite Generation

Hypochlorite was generated by bubbling chlorine gas through a cold solution of 5% sodium hydroxide.⁶ A Baird and Tatlock electrolytic analysis apparatus was also used for electrochemical generation of hypochlorite from alkaline sodium chloride. The arsenite method was used for the determination of the hypochlorite concentration in the sample.⁷

2.3. Kinetic Measurements

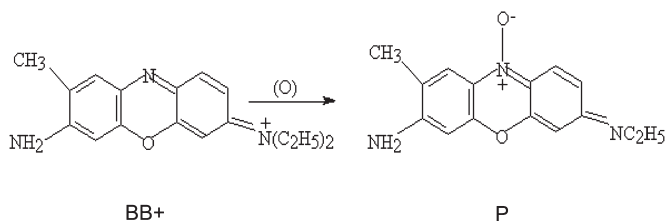
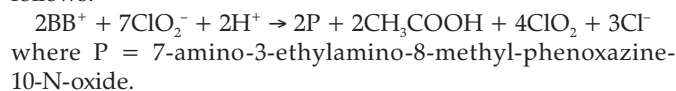
In all the experiments the *pseudo* first-order kinetics with respect to BB^+ were maintained and the reaction progress was monitored at 622 nm, using either a Cary-100 UV-VIS double-beam spectrophotometer or a HITECH SF61-DX2 micro-volume stopped flow apparatus at $25.0 \pm 0.1^\circ\text{C}$ unless otherwise specified. No interferences from the reagents, intermediates or products were observed at 622 nm. Reagent solutions were mixed in the order: requisite volumes of BB^+ , sulphuric acid, water plus other reagents, where necessary. In the experiments using the Cary 100, the total initial volume of the reaction mixture was always kept at 10 mL and a separately thermostatted solution of sodium chlorite was added to commence the reaction. After vigorous mixing, the solution was transferred to a thermostatted spectrophotometer cell.

2.4. Product Analysis and Stoichiometry

The product analysis of this reaction was carried out after mixing 250 mg of brilliant cresyl blue in 2.0 M H_2SO_4 in 250 mL

*To whom correspondence should be addressed. E-mail: jonnalagaddas@ukzn.ac.za

with 250 mg of NaClO₂ in 250 mL for 4 h. The organic component of the reaction mixture was extracted with diethyl ether and by thin layer chromatography (TLC); acetic acid was identified to be one of the products. The ether extract was taken to the rotavapor and concentrated. The TLC of the ether extract indicated two measure spots. Based on the TLC analysis the solvent system found to be most effective in separating these major products was 8:2 hexane:ethyl acetate. A silica packed column was used to separate the compounds. The major product was analysed using ¹H and ¹³C NMR. The major product has 15 carbon atoms, with heterocyclic structure intact and has ethylamino and methyl substituents in the 3 and 8 positions, respectively. The IR spectra of the sample showed an intense absorption peak between 1300 and 1200 cm⁻¹ indicating N-O stretching. No absorption bands in the range 3456–3407 cm⁻¹ and 1660–1641 cm⁻¹ were observed, excluding the formation of any carboxylic acid.⁸ Based on the IR spectra, the major product was identified as 7-amino-3-ethylamino-8-methyl-phenoxazine-10-N-oxide (P), which is further supported by high-resolution mass spectrometry (HRMS) which showed m/z 353 u (60%) and other major peaks at 340 u (40%) and 335 u (23%). N-oxide formation from the oxidation of pyridines and phenothiazines by hydrogen peroxide and other oxidizing agents has been reported in the literature.⁹ Studies on the further characterization of the reaction products are in progress. The stoichiometry was determined using 1:10 and 1:20 molar ratios of BB⁺ to chlorite and with excess of H⁺. After about 1 h, 2 h and 4 h incubation, the absorbances at 662 nm and 358 nm (ClO₂ formation) were measured and the residual oxidizing capacity was determined iodometrically by titrating with sodium thiosulphate using starch as an indicator. BB⁺ and chlorite ion react in the ratio of 2:3 with overall stoichiometric ratio as follows:



3. Results and Discussion

Under the excess concentration conditions of chlorite and acid, with [H⁺] = 0.10 M, [ClO₂⁻] = 0.05 M and [BB⁺] = 2.0 × 10⁻⁵ M, Figure 1 shows the repetitive scan spectra, depicting the depletion of brilliant cresyl blue at 622 nm and the accumulation of chlorine dioxide. ClO₂ is relatively inert at low pH and its formation is evident from the characteristic wavelike spectrum with a maximum at 358 nm.⁵ A plot of ln A at 622 nm *versus* time gave a straight line, which indicates that reaction under the chosen conditions follows *pseudo* first-order kinetics and the order with respect to [BB⁺] is unity.

3.1. Order with Respect to Chlorite and Hydrogen Ion

Under low acid conditions, the reaction rate was initially slow and it increased with time, showing autocatalytic behaviour. Such a non-linear trend was very pronounced when [chlorite] ≫ [H⁺]. In the current studies all the experiments were done with [H⁺] > [chlorite] and all the BB⁺ depletion curves showed exponential decay over two half-lives (see Fig. 2). Figure 3 shows typical absorbance *versus* time plots of formation of ClO₂ at fixed

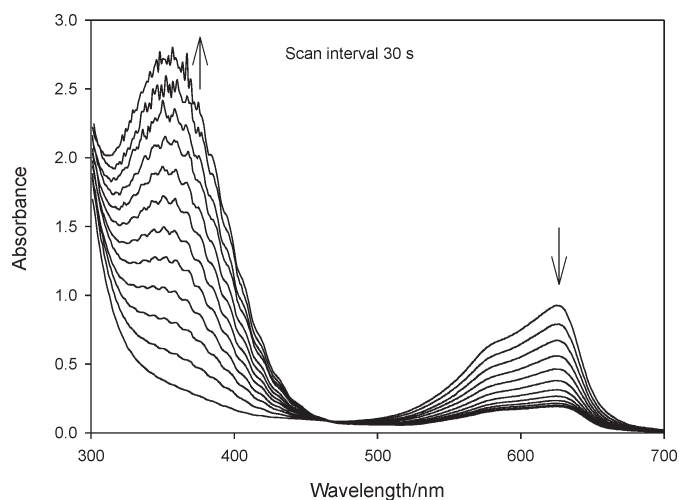


Figure 1 Repetitive scan spectra showing the depletion of brilliant cresyl blue (622 nm) and formation of chlorine dioxide (358 nm). [BB⁺] = 2.0 × 10⁻⁵ M, [H⁺] = 0.8 M and [ClO₂⁻] = 0.05 M at 25°C.

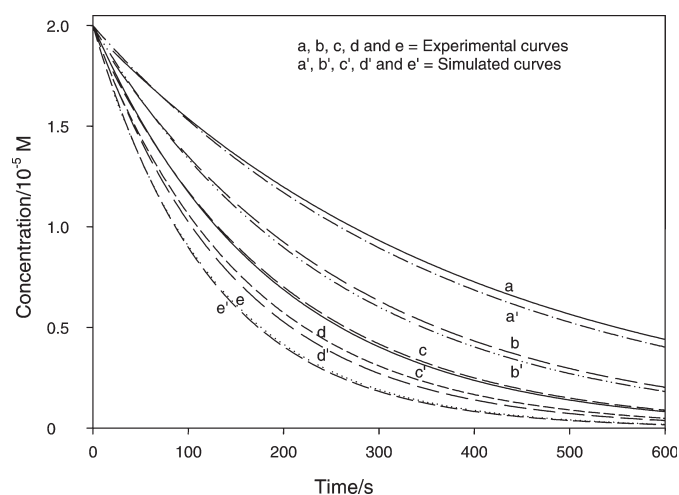


Figure 2 Effect of variation of chlorite concentration. Experimental and simulated curves showing the depletion of BB⁺ for different chlorite concentrations. [BB⁺] = 2.0 × 10⁻⁵ M, [H⁺] = 0.8 M and [ClO₂⁻] = (a) 0.02, (b) 0.03, (c) 0.04, (d) 0.05 and (e) 0.06 M at 25°C.

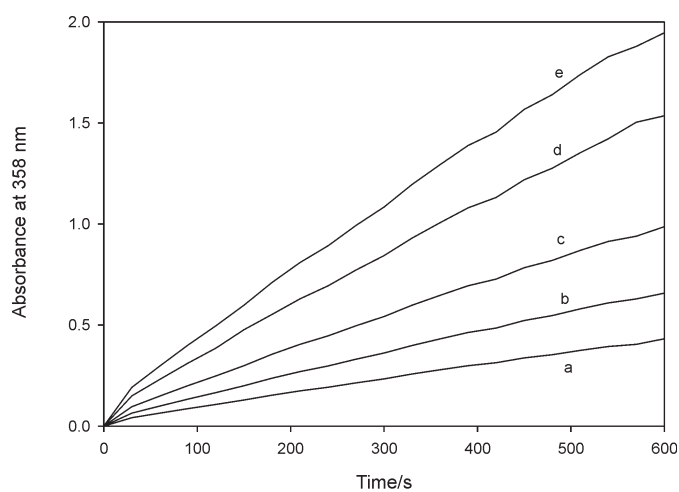


Figure 3 Effect of variation of chlorite concentration. Absorbance *versus* time plots showing the formation of ClO₂ for different chlorite concentrations. [BB⁺] = 2.0 × 10⁻⁵ M, [H⁺] = 0.8 M and [ClO₂⁻] = (a) 0.02, (b) 0.03, (c) 0.04, (d) 0.05 and (e) 0.06 M at 25°C.

Table 1 Variation of rate constants with respect to chlorite and acid concentrations. $[BB^+] = 2.0 \times 10^{-5}$ M. Temperature = $25.0 \pm 0.5^\circ\text{C}$. Kinetic data are average values of duplicate experiments with coefficient of variance <3%. Equation of plot of $\ln k_0'$ versus $\ln [\text{ClO}_2^-]$: $y = 0.9989x - 2.0721$, $R^2 = 0.9959$; equation of plot of $\ln k_0$ versus $\ln [\text{H}^+]$: $y = 0.9827x - 4.8555$, $R^2 = 0.9996$.

$[\text{ClO}_2^-]/\text{M}$	$[\text{H}^+]/\text{M}$	$k_0'/10^{-3}\text{ s}^{-1}$	$k_0/\text{l}^2\text{ mol}^{-2}\text{ s}^{-1\text{a}}$
I = 1.27 M			
0.02	0.8	2.54	0.159
0.03	0.8	3.75	0.156
0.04	0.8	5.17	0.162
0.05	0.8	6.19	0.155
0.06	0.8	7.76	0.162
Mean			0.159
Standard deviation			0.003
I = 1.25 M			
0.05	0.2	1.61	0.161
0.05	0.3	2.38	0.159
0.05	0.4	3.12	0.156
0.05	0.6	4.78	0.160
0.05	0.8	6.23	0.155
Mean			0.158
Standard deviation			0.002

^a Third-order rate constant, $k_0 = k_0'/[\text{H}^+][\text{ClO}_2^-]$.

acid and ionic strengths for varying chlorite concentrations. Table 1 summarizes the *pseudo* first-order constants, k_0' , obtained at constant ionic strength for varying initial concentrations of chlorite and H^+ ions. The plots of $\ln k_0'$ versus $\ln [\text{ClO}_2^-]$ and $\ln k_0'$ versus $\ln [\text{H}^+]$ gave straight lines with slopes 0.998 ($R^2 = 0.997$) and 0.986 ($R^2 = 0.996$), respectively, suggesting that the reaction has first-order dependence with respect to both chlorite and H^+ . For the probable rate law,

$$r = k[\text{H}^+][\text{ClO}_2^-][\text{BB}^+],$$

the mean third-order rate constant for the reaction was $(0.159 \pm 0.003)\text{ l}^2\text{ mol}^{-2}\text{ s}^{-1}$.

3.2. Catalysed Reaction Dynamics

With a view to finding good catalyst cations to enhance the rate of the title reaction, the effect of a wide range of cations was investigated. Interestingly, divalent cations of Ni, Co, Mn, Cu, Pb, Rh and Pd; trivalent cations of As, Cr, Al, Bi and Sb; tetravalent cations of Ce and Se; and Re(V) or W(VI) had little or no effect on the reaction rate. While Fe(III) had some catalytic effect, Ru(III) demonstrated significant catalysing ability. Considering the selectivity and sensitivity of the catalyst, hence the scope of the title reaction for kinetic-catalytic determination of Ru(III), the detailed kinetics of the Ru(III)-catalysed reaction were investigated.

With excess acid and chlorite, the Ru(III)-catalysed depletion of brilliant cresyl blue followed *pseudo* first-order kinetics. The plots of $\ln A$ versus time yielded good straight lines. With $[\text{BB}^+]_0 = 2.0 \times 10^{-5}$ M, $[\text{ClO}_2^-]_0 = 0.05$ M and $[\text{H}^+]_0 = 0.80$ M, the values of the *pseudo* first-order constant, k' , were determined for various initial Ru(III) concentrations. The plot of k' versus $[\text{Ru(III)}]_0$ gave a good straight line with slope = $4.8 \times 10^4\text{ l mol}^{-1}\text{ s}^{-1}$, intercept = $6.1 \times 10^{-3}\text{ s}^{-1}$ and $R^2 = 0.9987$ (Fig. 4). The intercept value agreed well with the rate constant for the uncatalysed reaction.

To establish the reaction orders with respect to chlorite and acid in the Ru(III)-catalysed reaction, experiments were conducted at constant ionic strength, with varying initial

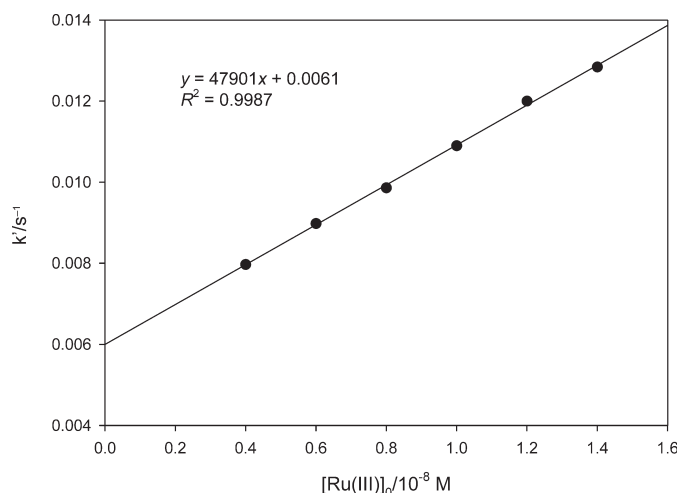


Figure 4 Effect of Ru(III) concentration on the reaction rate. $[\text{BB}^+] = 2.0 \times 10^{-5}$ M, $[\text{H}^+] = 0.8$ M and $[\text{ClO}_2^-] = 0.05$ M, $[\text{Ru(III)}] = (0.4 - 1.4) \times 10^{-8}$ M and I = 1.25 M. Temperature $25.0 \pm 0.5^\circ\text{C}$. Data are average values of duplicate experiments with coefficient of variance <3%.

concentrations of acid and chlorite. The $\ln k'$ versus $\ln [\text{ClO}_2^-]$ plot gave a slope of 0.986 with $R^2 = 0.99$, while the $\ln k'$ versus $\ln [\text{H}^+]$ plot gave a slope of 0.987 with $R^2 = 0.99$, suggesting that the reaction order is also unity with respect to both oxidant and acid in the catalysed reaction (Table 2). The third-order constant in presence of 1.0×10^{-7} M Ru(III) is $0.274 \pm 0.003\text{ l}^2\text{ mol}^{-2}\text{ s}^{-1}$. Based on the experimentally-established reaction orders for the Ru(III)-catalysed reaction, the catalytic constant, $k_{\text{CAT}} = k'/[\text{ClO}_2^-][\text{H}^+]$ was found to be equal to $(1.2 \pm 0.3) \times 10^6\text{ l}^3\text{ mol}^{-3}\text{ s}^{-1}$.

3.3. Effect of Ionic Strength, I

The role of the ionic strength on the dynamics of both the uncatalysed and Ru(III)-catalysed reactions was studied by measuring the rate constants for fixed concentrations of the reactants and varied amounts of the neutral salt, sodium sulphate. Figure 5 illustrates the plots of $\ln k_0'$ versus \sqrt{I} for both sets of experiments. When the ionic strength of the reaction mixture was increased from 0.65 M to 1.25 M, the uncatalysed reaction gave a slope of $-0.53\text{ l}^{1/2}\text{ mol}^{-1/2}$, while the catalysed reaction slope was $-0.45\text{ l}^{1/2}\text{ mol}^{-1/2}$ (Fig. 5). Both systems showed negative salt

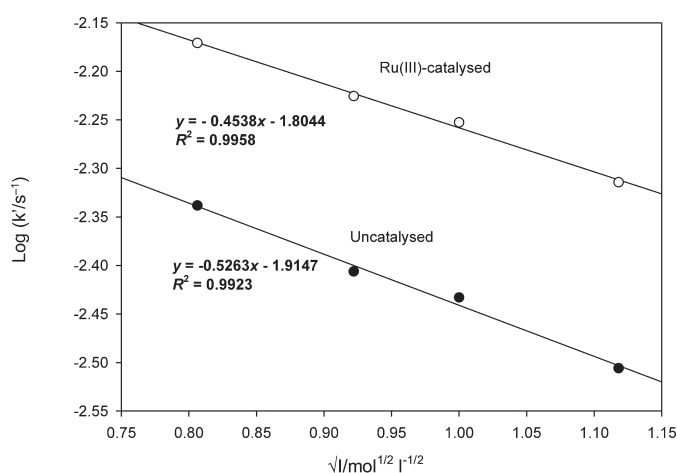
Table 2 Variation of rate constants with respect to chlorite and acid concentrations in Ru(III)-catalysed reaction. $[\text{BB}^+] = 2.0 \times 10^{-5}$ M, $[\text{Ru(III)}] = 1 \times 10^{-7}$ M, I = 1.25 M. Temperature = $25.0 \pm 0.5^\circ\text{C}$. Kinetic data are average values of duplicate experiments with coefficient of variance <3%. Equation of plot of $\ln k$ versus $\ln [\text{ClO}_2^-]$: $y = 0.9867x - 1.5611$; $R^2 = 0.999$; equation of plot of $\ln k$ versus $\ln [\text{H}^+]$: $y = 0.9871x - 4.2996$; $R^2 = 0.9988$.

$[\text{ClO}_2^-]/\text{M}$	$[\text{H}^+]/\text{M}$	$k'/10^{-3}\text{ s}^{-1}$	$k_{\text{CAT}}/\text{l}^2\text{ mol}^{-2}\text{ s}^{-1\text{a}}$
0.020	0.80	4.41	0.276
0.025	0.80	5.50	0.275
0.030	0.80	6.66	0.278
0.040	0.80	8.72	0.272
0.050	0.40	5.55	0.278
0.050	0.48	6.48	0.270
0.050	0.64	8.78	0.274
0.050	0.72	9.77	0.271
0.050	0.80	10.90	0.273
Mean			0.274
Standard deviation			0.003

^a $k_{\text{CAT}} = k'/[\text{H}^+][\text{ClO}_2^-]$.

Table 3 Effect of temperature on rate constants. $[BB^+] = 2.0 \times 10^{-5} \text{ M}$, $[ClO_2^-] = 0.05 \text{ M}$ and $[H^+] = 0.80 \text{ M}$.

Temperature /K	Uncatalysed		Catalysed: $[Ru(III)] = 1 \times 10^{-7} \text{ M}$	
	$k'/10^{-3} \text{ s}^{-1}$	$k/l^2 \text{ mol}^{-2} \text{ s}^{-1}$	$k'/10^{-3} \text{ s}^{-1}$	$k/10^6 \text{ l}^3 \text{ mol}^{-3} \text{ s}^{-1}$
293	4.91	0.123	8.20	2.05
298	6.31	0.158	9.42	2.36
303	9.39	0.235	11.80	2.95
308	12.21	0.305	14.72	3.68
313	15.65	0.391	17.21	4.30

**Figure 5** Effect of ionic strength on uncatalysed and Ru(III)-catalysed reactions. In k'_0 versus \sqrt{I} plots. Data are average values of duplicate experiments with coefficient of variance <3%. Uncatalysed reaction: $[BB^+] = 2.0 \times 10^{-5} \text{ M}$, $[H^+] = 0.4 \text{ M}$ and $[ClO_2^-] = 0.05 \text{ M}$; catalysed reaction: same conditions, with $[Ru(III)] = 1.0 \times 10^{-7} \text{ M}$.

effects, suggesting that the rate-limiting step involves oppositely charged species. Owing to the high ionic strengths of the reaction mixtures, the kinetic salt effect could only be assessed qualitatively.

3.4. Activation Energies

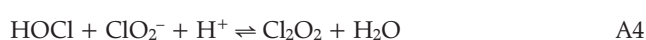
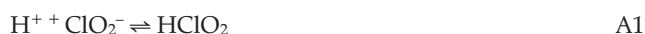
The energy parameters for both the uncatalysed and Ru(III)-catalysed reactions were studied by measuring the rate constants at different temperatures and by using the Arrhenius and Eyring equations (Table 3). Table 4 summarizes the calculated values of four activation parameters, namely the activation energies, enthalpies, entropies and frequency factors for both reactions. Both reactions had large negative entropies of activation, suggesting the formation of an activated complex, resulting in a decrease in entropy. Obviously, the catalysed reaction had a lower energy of activation of $29.4 \pm 0.9 \text{ kJ mol}^{-1}$ compared with $45.4 \pm 1.4 \text{ kJ mol}^{-1}$ for the uncatalysed reaction.

The stoichiometry of the overall reaction and the relative amounts of chlorine dioxide generated were observed to be dependent on the initial concentrations of reactants. Hence, the

Table 4 Arrhenius activation parameters. $[BB^+] = 2.0 \times 10^{-5} \text{ M}$, $[ClO_2^-] = 0.05 \text{ M}$ and $[H^+] = 0.80 \text{ M}$.

Property	Uncatalysed	Catalysed
Activation energy, $E_a/\text{kJ mol}^{-1}$	45.4 ± 1.4	29.4 ± 0.9
Frequency factor, $A/l^2 \text{ mol}^{-2} \text{ s}^{-1}$	$(1.5 \pm 0.4) \times 10^7$	
Frequency factor, $A/l^3 \text{ mol}^{-3} \text{ s}^{-1}$		$(3.5 \pm 1.4) \times 10^{11}$
Enthalpy of reaction, $\Delta H/\text{kJ mol}^{-1}$	38.0 ± 1.2	19.5 ± 0.6
Entropy of activation, $\Delta S/\text{J K}^{-1} \text{ mol}^{-1}$	-247 ± 7	-230 ± 7

impact of initial concentrations of acid, chlorite and chloride on the chlorine dioxide formation was investigated. A hundred-fold increase in added chloride concentration resulted in only a 20% increase in the amount of ClO_2 formed, while a four-fold increase in $[H^+]$ doubled the chlorine dioxide yield. A five-fold increase in chlorite concentration increased the amount of ClO_2 formed proportionately. This suggests that the initial concentration of chlorite has a profound effect on the ClO_2 formation, followed by acid and chloride with marginal effects. As chlorine dioxide is relatively inert at acidic pH, it accumulated continuously. The concentrations of ClO_2 were calculated using $\epsilon_{\text{max}} = 1250 \text{ l mol}^{-1} \text{ cm}^{-1}$ at $\lambda_{\text{max}} = 358.5 \text{ nm}$.⁵ Further, for fixed chlorite concentration, while the total amount of ClO_2 formed remained the same, its rate of formation increased with an increase in the initial concentration of BB^+ . This is obviously due to the limiting concentration of the dye, which is involved in the rate-determining step that controls the initial autocatalysed formation of HOCl and other chloro/oxychloro intermediates. For the current reaction conditions, i.e. at acidic pH, as chlorate does not form,¹⁰ the equations involving chlorate can be excluded from the mechanism. Based on a literature review, the chemistry of chlorite ion and other oxychloro species may be represented as follows^{11,12}



With increase in H^+ concentration, the amount of ClO_2 produced increases moderately. As the rate of reaction A5 is acid-dependent, an increase in H^+ concentration favours the rapid decomposition of Cl_2O_2 , resulting in autocatalytic formation of HOCl. Further, the increase in acid concentration also increases $[Cl_2]$ through the forward reaction of Equation A2. Chlorine is much more reactive than HOCl and facilitates more chlorine dioxide formation.¹³

3.5. Kinetics of Reaction between BB^+ and HOCl

Under acidic conditions, although the title reaction does not exhibit any autocatalytic behaviour, HOCl plays a vital role in the oxidations involving acidic chlorite. Therefore, the kinetics of the reaction between BB^+ and hypochlorous acid were studied under different pH conditions. To understand the reaction dynamics, a close look at the chemistry of hypochlorite is crucial. HOCl is a weak acid with $pK_a = 7.4$ and dissociation constant $K_a = 4.0 \times 10^{-8} \text{ mol L}^{-1}$, i.e. even at a basic pH of 7.4, the concentrations of hypochlorite and hypochlorous acid will be equal. Even very small acid concentrations will shift the equilibrium towards more HOCl.⁵ The preliminary experiments showed that at

Table 5 Rate constants as functions of hypochlorite and hypochlorous acid concentrations. $[BB^+] = 2.0 \times 10^{-5}$ M. pH = 8.5. Temperature = $25.0 \pm 0.5^\circ\text{C}$. Kinetic data are mean values of duplicate experiments with coefficient of variance <3%.

$[\text{OCl}^-]_T / 10^{-3}\text{M}$	$[\text{OCl}^-] / 10^{-3}\text{M}$	$[\text{HOCl}] / 10^{-3}\text{M}$	$k_1' / 10^{-2}\text{s}^{-1}$	k_2' / s^{-1}	$k_1^a / \text{l mol}^{-1}\text{s}^{-1}$	$k_2^b / 10^3 \text{l mol}^{-1}\text{s}^{-1}$
1.21	0.91	0.30	1.78	0.36	19.6	1.19
2.41	1.81	0.60	3.69	0.74	20.4	1.23
3.62	2.72	0.91	5.60	1.10	20.6	1.21
4.82	3.62	1.21	8.04	1.49	22.2	1.24
6.03	4.52	1.51	9.60	1.84	21.2	1.22
Mean					20.8	1.22
Standard deviation					0.09	0.07

^a $k_1 = k_1' / [\text{OCl}^-]$.^b $k_2 = k_2' / [\text{HOCl}]$.**Table 6** Rate constants as functions of hypochlorite and hypochlorous acid concentrations. $[BB^+] = 2.0 \times 10^{-5}$ M. Initial pH of OCl^- solution = 7.0. $[\text{OCl}^-]_T = 2.41 \times 10^{-3}$ M. Temperature = $25.0 \pm 0.5^\circ\text{C}$. Kinetic data are mean values of duplicate experiments with coefficient of variance <3%.

$[\text{H}^+] / 10^{-4}\text{M}$	$[\text{OCl}^-] / 10^{-4}\text{M}$	$[\text{HOCl}] / 10^{-3}\text{M}$	$k_1' / 10^{-2}\text{s}^{-1}$	$k_2' / 10^{-2}\text{s}^{-1}$	$k_1^a / \text{l mol}^{-1}\text{s}^{-1}$	$k_2^b / 10^3 \text{l mol}^{-1}\text{s}^{-1}$
0.0	9.67	1.44	2.11	1.89	21.8	1.31
1.0	8.67	1.54	2.05	2.01	23.6	1.30
2.0	7.67	1.64	1.60	2.08	20.9	1.27
3.0	6.67	1.74	1.50	2.23	22.5	1.28
4.0	5.67	1.84	1.30	2.31	22.9	1.25
5.0	4.67	1.94	1.01	2.49	21.4	1.28
7.0	2.67	2.14	0.55	2.68	20.6	1.25
Mean					21.5	1.26
Standard deviation					0.11	0.04

^a $k_1 = k_1' / [\text{OCl}^-]$.^b $k_2 = k_2' / [\text{HOCl}]$.

pH > 9, when the bulk of the oxidant is in the hypochlorite form, the reaction was very slow. The effect of varying the hypochlorite concentration on the reaction kinetics was hence studied at pH 8.5. Further, the effect of added acid on the reaction rate was also investigated using the stopped flow equipment. As the reaction rates were pH-dependent, and pH dropped with the progress of reaction, changes were of the order of 0.5 pH units near neutral/mild acidic conditions. A variety of buffers, including ammonium, borate, phthalate and phosphate were tried to buffer the systems. All these buffers significantly retarded the rates of the reactions. The kinetic salt effect could also have contributed to some extent to the sluggishness of the reactions. Even acetate buffer at high concentration had a retarding influence on the rate. Furthermore, as the addition of acid shifts the equilibrium towards formation of HOCl, the initial pH of the reaction mixture should be worked out based on the residual concentration of acid in the system. Hence, considering the implications, mild acetate buffer ($[\text{CH}_3\text{COONa}] = 0.005$ M) with appropriate amounts of acetic acid to match the pH with residual $[\text{H}^+]$ were used only in the near-neutral pH experiments. In the experiments conducted at pH 8.5 and at low pH, no buffers were used. The absorbance-time data were analysed for rate constants. Both under alkaline and mild acidic conditions, the kinetic data had a better fit with a bi-exponential equation,

$$y = A_1 \exp(-k_1 x) + A_2 \exp(-k_2 x) + Mx + C,$$

than with a simple first-order equation. This suggests the concurrent occurrence of two *pseudo* first-order pathways, i.e. a slow reaction initiated by hypochlorite (k_1') and the other initiated by HOCl (k_2'). With increase in added acid concentration, while the former constant decreased, the latter constant recorded an increase. The results obtained are summarized in

Tables 5 and 6. At pH 8.5, 25% of the total hypochlorite exists in the form of HOCl, increasing to 60% at pH 7, and 99% at pH 3. The relative amounts of hypochlorite and HOCl for different amounts of acid were calculated using the K_a for the fast equilibrium between H^+ , OCl^- and HOCl. A scrutiny of the overall second-order rate constants summarized in the last two columns of Tables 5 and 6 show that the rate constant of the HOCl-initiated reaction was much higher than for the hypochlorite-initiated reaction. At low pH (<3), only HOCl exists. Interestingly, a further increase in H^+ concentration increased the *pseudo* first-order rate constant proportionately, suggesting a first-order dependence of the reaction rate on acid concentration under these conditions (Table 7). The plot of k' versus $[\text{H}^+]$ gave a good straight line, with $R^2 = 0.997$, confirming that the order with respect to H^+ is unity at low pH conditions. The third-order rate constant is estimated to be $(2.31 \pm 0.06) \times 10^5 \text{ l}^2 \text{ mol}^{-2} \text{ s}^{-1}$.

Table 7 Rate constants at low pH. $[BB^+] = 2.0 \times 10^{-5}$ M. Initial pH of OCl^- solution = 7.0. $[\text{OCl}^-]_T = 2.60 \times 10^{-3}$ M. Temperature = $25.0 \pm 0.5^\circ\text{C}$. Kinetic data are mean values of duplicate experiments with coefficient of variance <3%. Equation of plot of k' versus $[\text{H}^+]$: $y = 601.9x + 0.045$, $R^2 = 0.9968$.

$[\text{H}^+] / \text{M}$	k' / s^{-1}	$k^a / 10^5 \text{ l}^2 \text{ mol}^{-2} \text{ s}^{-1}$
0.01	5.95	2.29
0.02	11.92	2.29
0.03	18.82	2.41
0.04	23.63	2.27
0.05	30.19	2.32
Mean		2.31
Standard deviation		0.06

^a $k = k' / [\text{H}^+][\text{HOCl}]$.

ming language. It allows the manual optimization of the estimated rate coefficients and provides an opportunity to plot the experimental and corresponding simulated curves simultaneously. Simkine uses Predictor-Corrector methods which are Gear's backward differentiation methods and the generalizations of the Bulirsch-Stoer methods, also called semi-implicit extrapolation methods (SIEM).²¹ SIEM methods, which use the modified midpoint rule²¹ are more stable at large step size and more efficient at small error tolerance. Table 8 summarizes the 11 reactions and their rate constants used for the simulation. For Equations R1 to R5 the respective rate constants were taken as reported in the literature,^{13,15} while the rate constants used for Equations R6 and R8 were the experimental results obtained from the current studies. The other values were the estimated values. The estimated values were adjusted to obtain curves which agreed with the experimental curves.

4. Conclusions

Figure 2 shows the simulated curves with varying initial concentrations of chlorite. They agree fairly well with the five experimental curves. The computed chlorine dioxide concentrations were lower than the values expected from the experiments. Probably, other reactions such as



which are not included in these simulations may have to be considered in the mechanism to improve the scheme. Further, Fig. 6 and its insert show the kinetic concentration profiles generated through the computation, for depletion of BB^+ and the formation and consumption of reaction intermediates together with the formation of reaction products. A good agreement between the experimental and simulated curves for BB^+ and a fair match in the trends in the simulated and experimental curves for ClO_2 support the plausibility of the proposed mechanism for the title reaction.

Acknowledgements

The authors thank the University of KwaZulu-Natal and the National Research Foundation, Pretoria, for funding the project and Professor F. Shode and Mr S. Naidoo, UKZN, for their help in product characterization.

References

- 1 M. Orban and I.R. Epstein, *J. Phys. Chem.*, 1982, **86**, 3907–3914.
- 2 I. Nagypal, G. Bazsa and I.R. Epstein, *J. Am. Chem. Soc.*, 1986, **108**, 3635–3641.
- 3 (a) T.W. Clapper and W.A. Gale, in *Encyclopedia of Chemical Technology*, (R.E. Kirk and D.F. Othmer, eds.), vol. 5, 2nd edn., John Wiley, New York, 1964. (b) G. Gordon, W.J. Cooper, R.G. Rice and G.E. Pacey, *Disinfectant Residual Measurement Methods*, AWWA Research Report, American Water Works Research Foundation, Denver, CO, 1987, and

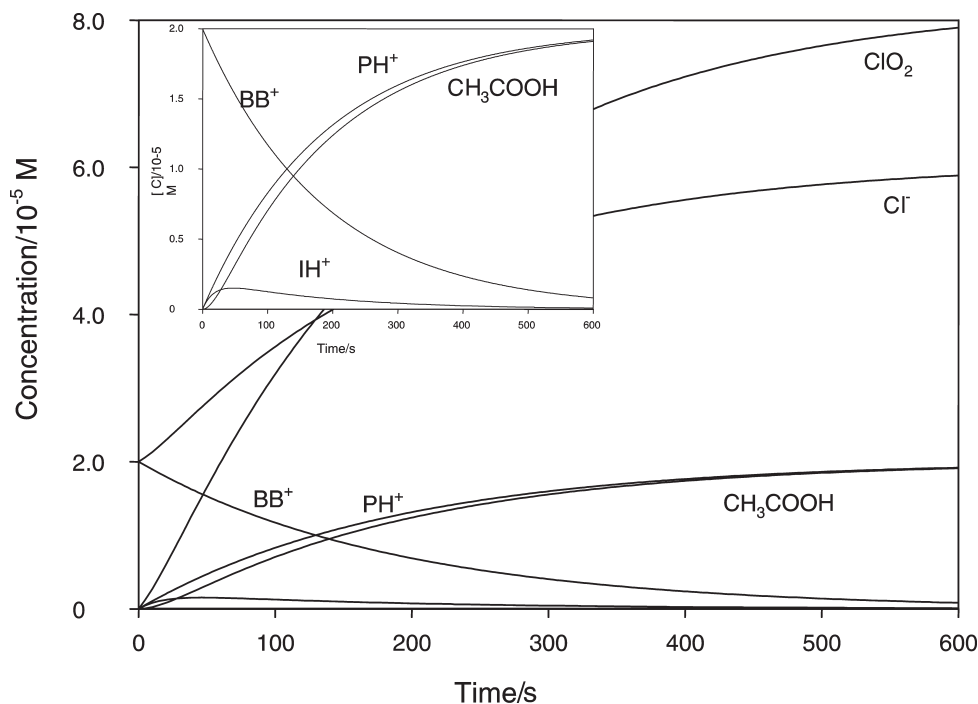


Figure 6 Computed curves showing the kinetic profiles of BB^+ , reaction intermediates and products. Conditions the same as in Figs 2 and 3, curve c.

references therein.

- 4 G. Clark, *Staining Procedures*, (E. Williams and K. Wilkins, eds.), Pergamon Press, Oxford, 1981.
- 5 (a) I. Fabian and G. Gordon, *Inorg. Chem.*, 1991, **30**, 3994–3999. (b) L.C. Adam, I. Fabian, K. Suzuki and G. Gordon, *Inorg. Chem.*, 1992, **31**, 3534–3540.
- 6 V. Chunilall, M. Govender and S.B. Jonnalagadda, *J. Env. Sci. Health*, 2002, **A37**(8), 1523–1531.
- 7 A.I. Vogel, *Textbook of Quantitative Inorganic Chemistry*, 3rd edn., Longmans Green, London, 1966.
- 8 J.G. Grasselli and J.W.M Ritchey, *Atlas of Spectral Data and Physical Constants for Organic Compounds*, vol. 1, 2nd edn., CRC Press, Cleveland, OH, 1975.
- 9 (a) R.C. Elderfield, *Heterocyclic Compounds*, vol. 6, John Wiley, New York, 1957. (b) L.A. Paquette, *Principles of Modern Heterocyclic Chemistry*, W.A. Benjamin, New York, 1968. (c) S.B. Jonnalagadda, M. Shezi and B. Pare, *Int. J. Chem. Kinetics*, 2003, **35**, 294–303.
- 10 C.F. Furmann and D.W. Margerum, *Inorg. Chem.*, 1998, **37**, 4321–4328.
- 11 G. Peintler, I. Nagypal and I.R. Epstein, *J. Phys. Chem.*, 1990, **94**, 2954–2961.
- 12 I.R. Epstein, K. Kustin and R.H. Simoyi, *J. Phys. Chem.*, 1992, **96**, 5852–5859.
- 13 R.G. Kieffer and G. Gordon, *Inorg. Chem.*, 1968, **7**, 235–244.
- 14 (a) M.A. Salem, C.R. Chinake and R.H. Simoyi, *J. Phys. Chem.*, 1996, **100**, 9377–9384, (b) C.R. Chinake, O. Olojo and R.H. Simoyi, *J. Phys. Chem.*, 1998, **102**, 606–611.
- 15 T. Naota, H. Takaya and S. Murahashi, *Chem. Rev.*, 1998, **98**, 2599–2510.
- 16 (a) W.A. Lee and T.C. Bruice, *J. Am. Chem. Soc.*, 1985, **107**, 513–518. (b) N. Kumiya, S. Nuji and S. Murahashi, *Chem. Commun.*, 2001, 65–70.
- 17 (a) T.D. Avtokratova, *Analytical Chemistry of Ruthenium*, Humphrey Science Publications, London, 1969. (b) A. Brahmaiah and P. Manikyamba, *Indian J. Chem.*, 1995, **34A**, 900–905.
- 18 W.P. Griffith, *Chem. Soc. Rev.*, 1992, **21**, 179–186 and references therein.
- 19 I. Fabian and G. Gordon, *Inorg. Chem.*, 1992, **31**, 2114–2150.
- 20 S.B. Jonnalagadda, N. Parumasur and M.N. Shezi, *Comp. Biol. Chem.*, 2003, **23**, 147–152.
- 21 W.H. Press, B.P. Flannery, S.A. Teukolsky and W.T. Vetterling, *Numerical Recipes: The Art of Scientific Computing*, 2nd edn., Cambridge University Press, New York, USA, 1992.